THE JOURNAL OF PHYSICAL CHEMISTRY B

B: Fluid Interfaces, Colloids, Polymers, Soft Matter, Surfactants, and Glassy Materials

Simulating Surfactant-Iron Oxide Interfaces: From Density Functional Theory to Molecular Dynamics

Carlos Ayestarán Latorre, James Patrick Ewen, Chiara Gattinoni, and Daniele Dini

J. Phys. Chem. B, **Just Accepted Manuscript** • DOI: 10.1021/acs.jpcb.9b02925 • Publication Date (Web): 11 Jul 2019

Simulating Surfactant-Iron Oxide Interfaces: From Density Functional Theory to Molecular Dynamics

Carlos Ayestarán Latorre,[†,¶] James P. Ewen,[*,†,¶] Chiara Gattinoni,[‡,†] and Daniele Dini[†]

†*Department of Mechanical Engineering, Imperial College London, London SW7 2AZ, UK*

‡*Department of Materials, ETH Zürich, Zürich 8092, Switzerland*

¶*These authors contributed equally to this work*

E-mail: j.ewen@imperial.ac.uk

Abstract

Understanding the behaviour of surfactant molecules on iron oxide surfaces is important for many industrial applications. Molecular dynamics (MD) simulations of such systems have been limited by the absence of a force-field (FF) which accurately describes the molecule-surface interactions. In this study, interaction energies from density functional theory (DFT) + U calculations with a van der Waals functional are used to parameterize a classical FF for MD simulations of amide surfactants on iron oxide surfaces. The Original FF, which was derived using mixing rules and surface Lennard-Jones (LJ) parameters developed for nonpolar molecules, were shown to significantly underestimate the adsorption energy and overestimate the equilibrium adsorption distance compared to DFT. Conversely, the Optimized FF showed excellent agreement with the interaction energies obtained from DFT calculations for a wide range of surface coverages and molecular conformations near to and adsorbed on α-$Fe_2O_3(0001)$.

This was facilitated through the use of a Morse potential for strong chemisorption interactions, modified LJ parameters for weaker physisorption interactions, and adjusted partial charges for the electrostatic interactions. The Original FF and Optimized FF were compared in classical nonequilibrium molecular dynamics (NEMD) simulations of amide molecules confined between iron oxide surfaces. When the Optimized FF was employed, the amide molecules were pulled closer to the surface and the orientation of the headgroups was more similar to that observed in the DFT calculations compared to the Original FF. The Optimized FF proposed here facilitates classical MD simulations of anhydrous amide-iron oxide interfaces in which the interactions are representative of accurate DFT calculations.

Introduction

An improved understanding of the behavior of surfactant molecules on iron oxide surfaces would benefit a range of applications; from stabilizing iron oxide nanoparticles for use as biomarkers and catalysts,[1] to extracting iron ore for steel production,[2] and to protecting steel surfaces for corrosion inhibition.[3] Another application where the surfactant-iron oxide interface is of particular importance are friction modifier additives to lubricate steel surfaces.[4] Friction modifiers are added to lubricants to reduce friction and wear in machine components,[4] increase the energy efficiency of engineering systems, and ultimately reduce fuel consumption and CO_2 emissions.[5]

Within this class of additives, organic friction modifiers (OFMs) are notable because they are based solely on C, H, O, and N atoms and are not environmentally harmful. OFMs are amphiphilic surfactant molecules that contain nonpolar aliphatic tailgroups attached to polar headgroups.[4] They adsorb to metal, metal oxide, ceramic, or carbon-based surfaces through their polar headgroups, and can eventually form high coverage monolayers.[6,7] These monolayers prevent the direct contact of opposing sliding surfaces due to van der Waals (vdW) forces between proximal nonpolar tailgroups.[4]

The majority of engine components are made from steel, which forms iron oxide surfaces when exposed to air.[8] Therefore, a wide range of experiments have been used to investigate the nanoscale structure of surfactant films on iron oxide surfaces;[4] from polarized neutron reflectometry (PNR)[7] to the quartz crystal micro-balance (QCM).[9] The nature and strength of surfactant adsorption on iron oxide has also been investigated through FTIR,[10,11] X-ray photoelectron spectroscopy (XPS)[10,12,13] and polarization modulation-infrared reflection absorption spectroscopy (PM-IRRAS)[13] experiments. Moreover, the friction of surfactant films on iron oxide surfaces has been studied experimentally at both the nanoscale[14] and the macroscale.[4,15]

In addition to these experimental studies, classical molecular dynamics (MD) simulations have given unique insights into the nanoscale behaviour of OFM additive films.[16] For example, Doig et al.[17,18] and Ewen et al.[19–21] have used MD simulations to investigate the nanoscale structure and friction behavior of a range of OFM molecules on α-Fe_2O_3 surfaces. The accuracy of all MD simulations is heavily dependent on the force field (FF) used to describe the interatomic interactions.[20,22,23] Significant effort has been devoted to parameterizing FFs to accurately reproduce the bulk thermodynamic properties of a wide range of organic liquids.[24–29] However, relatively fewer FFs have been parameterized to accurately represent the interactions between organic molecules and solid surfaces.[30] In MD simulations, the interfacial vdW and electrostatic interactions are usually represented through Lennard-Jones (LJ)[31] and Coulomb potentials. For example, INTERFACE-FF[32] provides LJ and partial charge parameters as a transferable extension for the non-bonded interactions between organic liquids (using OPLS,[24] CHARMM,[28] AMBER,[27] etc.) and several silicate, aluminate, metal, oxide, sulfate, and apatite surfaces; however, no parameters for iron oxide were included. Similarly, CLAY-FF[33] includes LJ and partial charge parameters for many metal hydroxide, oxyhydroxide, and clay surfaces, including iron oxides. However, these parameters were developed primarily to model water adsorption and the suitability of ClayFF for interactions at the surfactant-iron oxide interface has not been tested. Previous

MD simulations of surfactant-iron oxide systems[9,17–21] have thus relied upon the use of mixing rules from LJ and partial charge parameters that were developed for the adsorption of n-alkanes.[34,35]

First principles calculations, such as density functional theory (DFT), can be used to accurately determine the nature and strength of the interactions between molecules and surfaces.[36–40] Optimal parameters can be developed to match interaction energies, E_{int}, obtained from accurate DFT calculations in so-called interface FFs.[30] Interface FFs have been developed to facilitate accurate classical MD simulations of several molecules on iron oxide surfaces; for example, water[41] n-alkanes,[42] and refrigerants.[43] However, no interface FF has been developed for surfactant molecules on iron oxide surfaces.

Recent DFT calculations[40] have provided crucial insights into the interactions between surfactants (carboxylic acid, amide, mono-glyceride) and α-Fe_2O_3(0001) surfaces. Specifically, all of these surfactants were found to strongly chemisorb on the iron oxide surface. The carboxylic acid and glyceride molecules readily dissociated through the formation of a surface hydroxyl group, which would complicate the development of a classical FF for MD simulations. Conversely, the amide remained intact, making it a simpler target molecule for interface FF parameterization. In this study, an amide-iron oxide interface FF will be parameterized to match E_{int} values obtained from previous[40] and new DFT calculations of a wide range of amide surface coverages and molecular conformations near to and adsorbed on α-Fe_2O_3(0001). Starting from an Original FF using parameters from the literature,[34] important parameters will be modified, and some interactions overhauled, to maximize agreement with the accurate DFT calculations.

The interface FF is expected to be useful for classical MD simulations of a wide range of applications where amide-iron oxide interactions are important, such as; stabilizing nanoparticles,[1] extracting iron ore,[2] corrosion inhibition,[3] and lubrication.[4] As a final validation, the Optimized FF will be compared to the Original FF in large-scale NEMD simulations to investigate the structure, flow, and friction of amide films on iron oxide surfaces.[19] Studying

the nanoscale structure of the absorbed films shows that the orientation of the headgroup changes and the molecules are drawn closer to the surface when the Optimized FF is employed. However, for the preformed films studied here, which cannot be squeezed out of the contact, the flow and friction behaviour is only slightly affected, which validates previous work which used the Original FF.[17–21]

Methodology

The methodology for the DFT calculations will be discussed first, followed by details of the parameterization of the Optimized FF, and finally utilization of the Optimized FF in large-scale NEMD simulations.

DFT calculations

Procedure

The procedure for the DFT + U calculations was outlined in one of our recent publications.[40] Therefore, only the most important aspects of the methodology are given here, while full details can be found in Ref.[40]

The VASP software[44–46] was used with the projector augmented wave (PAW) method[47] and spin polarization. For Fe, 8 electrons were treated as valance electrons, 6 for O, 4 for C, 7 for N, and 1 for H. A non-local correlation functional was employed which includes vdW interactions; optB86b-vdW.[48,49] This vdW functional has been shown to perform extremely well in a wide range of molecular adsorption studies.[36–39] The plane-wave expansion was cut off at 550 eV and a Monkhorst-Pack k-points mesh of 4 x 4 x 1 was used for the slab systems. A Hubbard $U - J = 4$ eV (in the Dudarev approach)[50] was added to account for electronic correlations in the Fe 3d orbitals. This U correction results in a band gap of 1.98 eV for α-Fe_2O_3, which is within the experimentally observed range (1.9-2.2 eV).[51] Periodic boundary conditions are employed in the x- and y-directions[52] while 15 Å of vacuum was added in

the z-direction to prevent interactions between neighboring cells. A dipole correction was also used in the z-direction.[52]

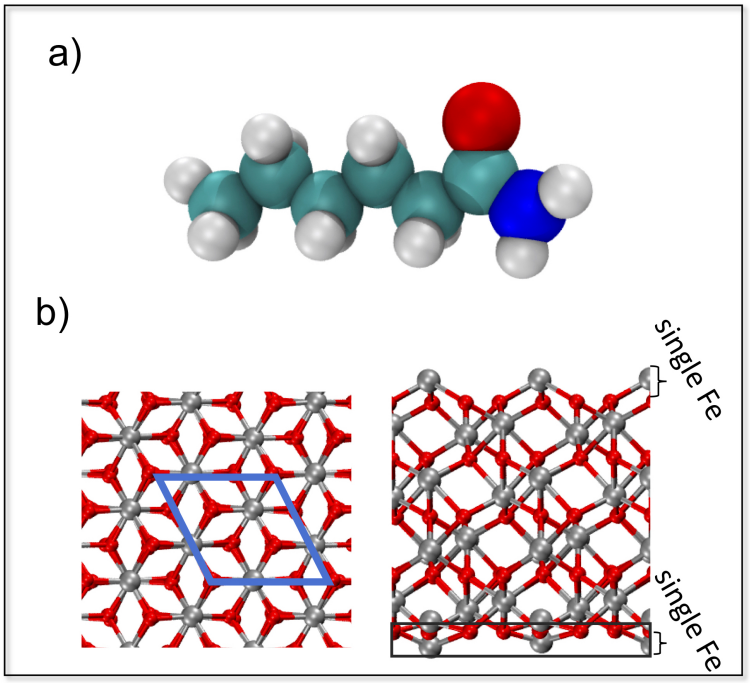

Figure 1: a) The surfactant molecule considered for the parameterization, hexanamide (HAm). b) Top (left) and side (right) view of the single Fe-terminated slab to represent the substrate for the adsorption calculations. O is shown in red and Fe in gray. In the left panel the blue box indicates the unit cell. The black box in the right panel shows the layers which are kept fixed. Visualized with VMD.[53]

A single Fe-terminated α-$Fe_2O_3(0001)$ slab (shown in Fig. 1) was selected as a representative model for the surface of steel. This has been shown by numerous theoretical and experimental studies to be the most stable termination of α-Fe_2O_3 at room temperature.[54] The α-$Fe_2O_3(0001)$ surface[42] as well as the α-$Fe_2O_3(00\bar{1}2)$ surface[43] have been used in recent FF parameterization studies. In tribology experiments, it is possible that the outer layer of α-$Fe_2O_3(0001)$ will become hydroxylated[55] due to water contamination of the lubricant.[56] However, XPS experiments have shown that surface hydroxyls can be displaced by long-chain carboxylic acids and amines on iron oxide surfaces.[57] Indeed, FTIR and XPS experiments of carboxylic acid OFMs indicated that a mixture of direct carboxylate-Fe_{surf} bonding and carboxylate-OH_{surf} H-bonding occurs at the α-Fe_2O_3-water interface.[11] Moreover, XPS ex-

periments of carboxylic acid[10,13] and amine[12] OFMs at the α-Fe_2O_3-oil interface showed that carboxylate-Fe_{surf} and dative N_{amine}-Fe_{surf} bonding are the dominant interactions in these cases. These observations suggests that direct OFM-Fe bonding (*via* inner sphere complexes[58]) predominate for OFM adsorption at the α-Fe_2O_3-oil interface. Previous DFT calculations on α-Fe_2O_3(0001) surfaces have shown a similar adsorption energy for amide OFMs and carboxylic acid OFMs,[40] so direct OFM-Fe_{surf} bonding can also be reasonably expected. Thus, although the steel used experimentally will present a range of surfaces terminations,[8] the selected system should be sufficient to capture the key interactions governing amide adsorption at oil-steel interfaces.

Amide headgroups were chosen since they are commercially relevant and do not readily dissociate on α-Fe_2O_3(0001) surfaces.[40] The tailgroups in most commercial OFMs are aliphatic chains containing 12-20 carbon atoms, mainly because they are readily available from natural fats, are soluble in most base oils, and significantly reduce friction.[4] Using molecules of this size would be prohibitively expensive from a computational perspective given the large number of DFT calculations required during this study. Since the focus here is the interaction of the headgroups with the surface, the saturated tailgroups are the minimum length to ensure that the geometry and partial charges within the headgroups are representative of molecules with longer tails. Tests in our previous DFT study[40] indicated that C_6 groups are sufficient to achieve this, so the parameterization was performed for hexanamide (HAm), as shown in Fig. 1.

Two surface coverages of HAm molecules were considered, which can be quantified by the number of molecules per area of surface, Γ. Specifically, a low coverage (LC) of $\Gamma \sim 1$ nm^{-2} and a high coverage (HC) of $\Gamma \sim 4$ nm^{-2}. Our previous DFT study showed that at HC, when the molecules in the monolayer are closely packed, they tend to adsorb almost vertically due vdW stabilization between neighboring tailgroups.[40] Conversely, molecules prefer to adsorb flat with the tailgroups almost parallel to the surface at LC.[40] An accurate representation of vdW forces is crucial to reproduce such behavior and tests in our previous study[40] showed

that the vdW interactions between two pentane molecules (models for the tailgroups) with the optB86b-vdW functional[48,49] were within 3% of the MP2-calculated values.[59]

In total, 29 different DFT configurations were employed in the training dataset for the parameterization. The most stable relaxed structures for HAm at LC (flat), LC (vertical), and HC were taken from Ref.[40] These configurations and the corresponding values of the adsorption energy, E_{ads}, from DFT are shown in Fig. 2.

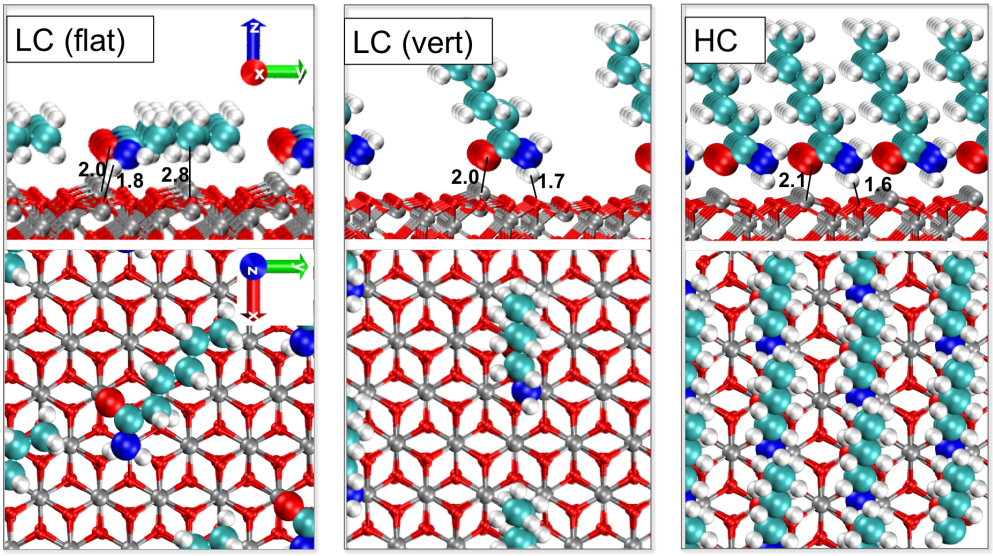

Figure 2: Side and top view of the most stable adsorption structures from Ref.[40] Adsorption energy, E_{ads} = -60.4 kcal mol^{-1} for LC (flat), -48.9 kcal mol^{-1} for LC (vertical), and -51.7 kcal mol^{-1} for HC. Marked distances between atom pairs are in Å. Visualized with VMD.[53]

Relaxed adsorption configurations, which showed slightly weaker adsorption compared to those included in Ref.,[40] as shown in the SI (Fig. S1), were also included in the training dataset to prevent overfitting.[60,61] These relaxed adsorption structures were further supplemented by systems in which the molecules were translated and/or rotated to ensure extensive sampling of the conformational phase space.[30] Specifically, single-point DFT calculations were performed with the HAm molecules translated in the direction perpendicular to the surface (z-scan) by 1.0 Å to 3.6 Å.[41,62–64] These calculations were performed on both the LC (flat) and LC (vertical) systems, to ensure that the E_{int}-distance profiles are accurately described by the Optimized FF for both cases. Single-point DFT calculations were also

performed on tilted conformations as intermediates between the flat and vertical cases.[62]

Since n-alkanes are also frequently included in large-scale NEMD simulations of amide-iron oxide systems,[19] E_{ads} was also calculated for n-hexane on α-Fe_2O_3(0001). In the most stable n-hexane adsorption structure obtained by structural relaxation, E_{ads} = -28.4 kcal mol^{-1}, as shown in the SI (Fig. S2). This represents relatively stronger adsorption than observed in previous DFT calculations of n-butane on α-Fe_2O_3(0001) which used vdW correction methods[42] rather than the vdW functional employed here.[48,49] The n-hexane molecule in the relaxed configuration was also translated in the z-direction to obtain a z-scan of E_{int} for this system. Since the focus of this interface FF is the behaviour of surfactants on iron oxide, the n-hexane results were used to ensure comparable performance to other FFs,[33–35] rather than forming part of the parameterization; as shown in the SI.

Interaction energy

The molecule-surface E_{int} was calculated by:[40]

$$E_{int} = (E_{sys} - E_{surf} - N_{mol} \times E_{mol})/N_{mol} \quad (1)$$

where E_{sys} is the total energy of the adsorbed system, E_{surf} is the total energy of the α-Fe_2O_3(0001) slab, E_{mol} is the total energy of the gas-phase molecule and N_{mol} is the number of HAm molecules in each cell. A negative value of E_{int}, therefore, indicates an energetically favorable interaction with respect to the isolated molecules and surface.

Interface force-field parameterization

Original force-field

The use of accurate all-atom FFs is critical to accurately reproduce the viscosity of bulk organic liquids[20,22] as well as the structure and friction of adsorbed monolayers.[20,65] Here, we use the optimized potentials for liquid simulations all-atom (OPLS-AA) FF,[24,25] which

includes parameters for the N, O, C, and H atoms in the amide headgroups.[19] For C and H atoms in the tailgroups and *n*-hexadecane molecules, updated parameters from L-OPLS-AA FF[26] are employed. L-OPLS-AA is a refinement of OPLS-AA specifically for long-chain alkanes, which significantly improves the agreement with experimental density and viscosity values for such molecules.[20] The bonded and non-bonded parameters for the interactions between the amide and *n*-hexadecane molecules are not changed during the parameterization. Thus, only non-bonded interfacial interactions between atoms in the amide molecules with the iron oxide surface atoms are directly parameterized.[41–43] In most FFs, such interactions are described using the 12-6 LJ[31] and Coulombic pair potentials:[30,32]

$$E_{non-bonded} = E_{LJ} + E_C = \sum_{i,j>i} \left[4\epsilon_{ij} \left[\left(\frac{\sigma_{ij}}{r_{ij}} \right)^{12} - \left(\frac{\sigma_{ij}}{r_{ij}} \right)^{6} \right] + \frac{C q_i q_j}{r_{ij}} \right] \quad (2)$$

where C is an energy-conversion constant, q_i and q_j are the partial charges of atoms i and j, r_{ij} is the distance between atoms i and j, ϵ_{ij} is the depth of the LJ potential well between atoms i and j, σ_{ij} is the distance at which the inter-particle LJ potential is zero. Each atom type is assigned unique q, ϵ, and σ parameters.

As a starting point (Original FF), LJ and partial charge parameters for the Fe_{surf} and O_{surf} atoms ($\epsilon_{Fe} = 2.5 \times \epsilon_O$) were taken from the FF due to Berro et al.[34] LJ interactions between dissimilar atoms are obtained using geometric mean mixing rules; $\sigma_{ij} = \sqrt{\sigma_i \sigma_j}$, $\epsilon_{ij} = \sqrt{\epsilon_i \epsilon_j}$, as specified for the OPLS-AA FF.[24] The choice of this FF over ClayFF[33] and the FF due to Savio et al.[35] is rationalized in the SI (Fig. S3). The LJ and partial charge parameters in the Original FF were developed to model the interactions between *n*-hexadecane molecules and Fe_2O_3 surfaces.[34] They have also been applied in several large-scale MD simulations of surfactant-iron oxide systems.[9,17–21]

Interface force-field optimization procedure

The atomic coordinates from the DFT calculations were transferred into LAMMPS[66] where the energy calculations for the Original FF and Optimized FF were performed. This was

facilitated using the Materials and Processes Simulations (MAPS) platform from Scienomics SARL. As for the DFT calculations, periodic boundary conditions were applied in x and y directions, with 15 Åof vacuum added in the z direction. The DFT systems were replicated three times in the x and y directions to prevent the molecules from interacting with their own periodic images.[43] A cutoff of 12 Å was used for the LJ interactions. A slab implementation of the particle-particle particle-mesh algorithm with a relative force accuracy of 10^{-5} was used for the electrostatic interactions.[67] Bonded and non-bonded interactions between the HAm molecules were described by the L-OPLS-AA FF.[24–26]

The Optimized FF parameters were obtained using a particle swarm algorithm.[68] The use of a minimization algorithm provides a more systematic and efficient method compared to the trial-and-error approaches commonly used for interface FF parameterization.[41,42] Quasi-Newtonian algorithms, which have been used in other interface FF parameterization studies[43] and have been implemented in some parameterization software packages[61,69] were also tested. However, such methods require accurate initial guesses since they are more suited to finding local minima. Conversely, particle swarm optimization can locate global minima;[68] a full description of this algorithm is given in the SI. The optimization was performed using relative deviations in E_{int} to the DFT values, as opposed to absolute deviations to ensure that geometries with lower E_{int} (and the lower associated absolute errors) were given equal weight.[30] Force-matching[70,71] was also included in the optimization for the relaxed DFT configurations, as described in the SI.

Initially, standard 12-6 LJ and partial charge parameters were optimized, but this approach proved insufficient to represent the strong interactions observed in the DFT calculations. An extensive analysis of different potential combinations is discussed in the SI. Ultimately, a combination of 12-6 LJ, Coulombic, and the Morse potential for the chemisoprtion interactions provided an excellent match to the DFT-calculated E_{int} values for the wide range of configurations considered.

Morse interactions

The DFT calculations in Ref.[40] showed that for HAm molecules on α-$Fe_2O_3(0001)$ surfaces, $E_{ads} \approx -50$ kcal mol^{-1}. Strong interactions between the oxygen atoms (O_{amide}) and nitrogen atoms (N_{amide}) in the amide headgroups with the surface iron atoms (Fe_{surf}) as well as between the headgroup hydrogen atoms (H_{amide}) and the surface oxygen atoms (O_{surf}) were observed. Fig. 3 shows that the O_{amide}-Fe_{surf}, N_{amide}-Fe_{surf}, and H_{amide}-O_{surf} interactions all involve charge transfer between the headgroup and the surface atoms, which is indicative of chemisorption.[40]

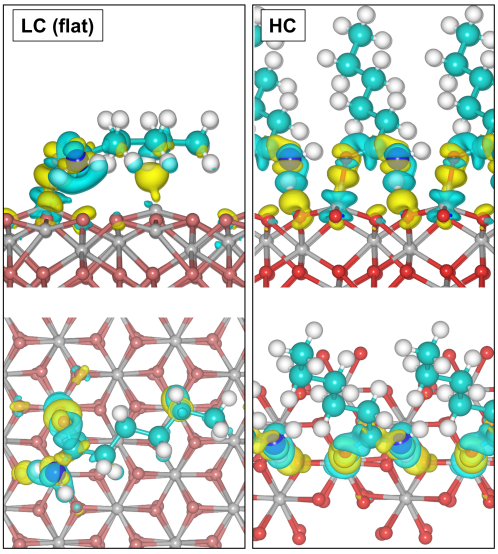

Figure 3: Side and top view of the electron density difference plots for the most stable low coverage (LC) and high coverage (HC) structures of HAm. Green represents regions of charge density depletion, while yellow represents regions of accumulation. The isosurface level is 0.003 e a_0^{-3} (where a_0 is the Bohr radius).

The 12-6 LJ potential used in the majority of classical FFs is better suited to reproducing weaker physisorption interactions.[62,63] Indeed, tests in which the surface LJ parameters and partial charges were modified from the Original FF showed only marginal improvement, as shown in the SI (Fig. S4-5). Therefore, to significantly improve the agreement between the Optimized FF and the DFT calculations, it was necessary to change the functional form of the O_{amide}-Fe_{surf}, N_{amide}-Fe_{surf}, and H_{amide}-O_{surf} interactions. Much better agreement

between the E_{ads} values from DFT calculations and the Optimized FF was obtained when the Morse potential was fit for these interactions:

$$E_{Morse_{ij}} = D_{ij}\left[e^{-2\alpha_{ij}(r_{ij}-r_{ij}^0)} - 2e^{-\alpha_{ij}(r_{ij}-r_{ij}^0)}\right] \quad (3)$$

where D_{ij} is the well depth, r_{ij}^0 is the equilibrium distance and α_{ij} determines the width of the potential.[72] The three tunable parameters allows the Morse potential to have both a deep potential well to reproduce strong short-range binding, but also decay in a manner consistent with the DFT calculations. This is not possible with LJ potentials which have a fixed $\sim r^{-6}$ decay and only two tunable parameters.[60] Moreover, the $1/r^{12}$ repulsion used in LJ is used primarily for numerical convenience, while the exponential repulsion in the Morse potential has more physical motivation.[70] Indeed, the Morse potential has been shown to more accurately reproduce E_{ads} from DFT compared to LJ potentials for a wide range of molecules on solid surfaces, for example; α-olefins (ethene to 1-decene) on Al(001) surfaces,[70] 1,4-bis(cyanophenyl)22,5-bis(decyloxy)-benzene on KCl(100),[60] gases (H_2, O_2, N_2, CO, H_2O, H_2S) on alkali metal-doped carbon nanotubes,[63] and water on Au(111).[64] Of particular relevance to this study, Morse interactions have also been used to accurately represent the S-Au chemisorption interactions of thiol molecules on Au surfaces.[73,74]

Optimized FF parameters

In the Optimized FF, nine parameters were fitted to Morse potentials to represent the strong O_{amide}-Fe_{surf}, N_{amide}-Fe_{surf}, and H_{amide}-O_{surf} interactions. Since the interactions between the remaining atom type pairs in the surface and HAm were of a physical rather than chemical nature, they were simultaneously fitted with a 12-6 LJ potential. It was sufficient to only change the surface LJ parameters and use geometric mean mixing rules for these weaker interactions rather than fitting each atom pair individually,[43] so this only added four parameters to the fitting. Note that the LJ interactions are ignored for the O_{amide}-Fe_{surf}, N_{amide}-Fe_{surf}, and H_{amide}-O_{surf} interactions in the Optimized FF. The partial charges of

the Fe_{surf} and O_{surf} atoms were also adjusted to maximize agreement with the E_{ads} values from the DFT calculations. A charge neutrality constraint was imposed on the surface (Fe:O charge ratio = 3:2), so only one additional parameter was required to determine the Fe_{surf} and O_{surf} partial charges. In total, 14 parameters were included in the fitting procedure.

The final parameters for the Optimized FF are presented in Table 1. The parameters are in general agreement with those developed previously for other molecular adsorption systems. The Morse parameters for the O_{amide}-Fe_{surf} and N_{amide}-Fe_{surf} are broadly similar to those developed for S-Au interactions of thiol molecules on Au surfaces.[73,74] Experimental values of E_{int} are not available for amides; however, XPS experiments of amines showed that dative N_{amine}-Fe_{surf} bonding dominates the interactions,[12] while carboxylate-Fe_{surf} bonding did so for carboxylic acids.[10,13] MP2 level calculations have shown that $E_{int} \approx 5$ kcal mol^{-1} for amide-water H-bonds (when water is the H-bond acceptor),[75] which is similar to the H_{amide}-O_{surf} Morse parameters used here. The LJ and partial charge parameters are only slightly changed from those used in the Original FF[34] (see Table S1).

Table 1: Final LJ, Morse and partial charge parameters for Optimized FF

	ϵ / kcal mol^{-1}	σ / Å	q / e
*Surface LJ**			
Fe_{surf}	0.28	2.09	0.645
O_{surf}	0.25	2.41	−0.430
	D / kcal mol^{-1}	r_0 / Å	α / Å^{-1}
Morse			
O_{amide}-Fe_{surf}	17.79	2.16	1.64
N_{amide}-Fe_{surf}	10.80	2.61	2.78
H_{amide}-O_{surf}	3.00	1.98	2.15

*Parameters for HAm remain unmodified from L-OPLS-AA,[24–26] and the remaining LJ parameters are determined by geometric mean mixing rules.

Large-scale NEMD simulations

Simulation set-up

As a final validation, the Optimized FF was tested in large-scale confined NEMD simulations of amide films adsorbed on α-Fe_2O_3 surfaces, separated by a thin layer of n-hexadecane. In previous simulations of similar systems,[17–21] the molecule-surface interactions were represented by LJ and Coulomb potentials, with the α-Fe_2O_3 surface parameters taken from Berro et al.[34] In this section, this Original FF (Table S1) will be compared to the Optimized FF (Table 1) in large-scale NEMD simulations. The L-OPLS-AA[24–26] FF was used to represent interactions between the amide and n-hexadecane molecules.

The simulation procedure is similar to that described in one of our previous studies.[19] Therefore only the most important details are included here, while the full methodology can be found in Ref.[19] The systems consist of a thin layer of n-hexadecane lubricant confined between amide films adsorbed on two α-Fe_2O_3(0001) slabs with x, y, z dimensions of $55, 55, 12$ Å. Periodic boundary conditions were applied in the x and y directions, so the amide or n-hexadecane molecules could not be squeezed out of the contact.[76]

The NEMD simulations were performed using LAMMPS,[66] and the equations of motion were integrated with the velocity Verlet algorithm with a time step of 1 fs. Fast-moving bonds involving hydrogen atoms were constrained with the SHAKE algorithm.[77] The α-Fe_2O_3 slab atoms were restrained by harmonic bonds between atoms within 3 Å, with a force constant of 130 kcal mol^{-1} Å^{-1}.[34]

Stearamide (SAm), which has a C_{18} tailgroup rather than C_6 tailgroup in HAm, was used since it is more representative of commercial OFMs.[4] SAm molecules were placed 3 Å from both of the solid surfaces prior to energy minimization. This is similar to the use of preformed Langmuir-Blodgett films in friction experiments.[78] Three different surface coverages of SAm were considered. A HC, where $\Gamma = 4.32$ nm^{-2} (close to the maximum theoretical value);[79] a MC, where $\Gamma = 2.88$ nm^{-2} ($\sim 2/3$ maximum); and a LC, where $\Gamma = 1.44$ nm^{-2} ($\sim 1/3$

maximum). 70 n-hexadecane molecules, equivalent to two molecular layers, were randomly inserted between the SAm films. This has been shown in previous squeeze-out simulations to be representative of the amount expected between OFM films under boundary lubrication conditions at 0.5 GPa.[19]

Simulation Procedure

The large-scale NEMD simulations consisted of three phases; minimization, compression and sliding. Starting with a density similar to that of liquid n-hexadecane (0.75 g cm^{-3}), the system was energy minimized. The system was then pressurized (0.5 GPa) and it was thermostatted (300 K) in the directions perpendicular to the compression and shear directions. Temperature was maintained with a Langevin thermostat with a relaxation constant of 0.1 ps.[80] Pressure was applied by adding a constant force to atoms in the outermost layer of the top slab, while keeping the outermost layer of atoms in the bottom slab fixed in the z direction. The systems were compressed for 500 ps, which was sufficient for the slab separation to reach a constant average value.

A velocity of $v = \pm 10$ m s^{-1} was added to the outermost layer of atoms in each slab such that $v_s = 20$ m s^{-1}. Four independent NEMD simulations were run for each coverage/FF combination, with the top slab sliding in the x, $-x$, y and $-y$ directions to account for potential friction anisotropy.[81] The sliding simulations were conducted for approximately 1 ns which was sufficient to reach a nonequilibrium steady state. Any heat generated during the sliding was dissipated using a thermostat acting only on the middle 10 Å of the α-Fe_2O_3 slabs, applied only in the y-direction (perpendicular to both the sliding and compression). This approach ensures that the dynamics of the confined liquids molecules is not unphysically influenced under sliding conditions.[82] Using this thermostatting method, the temperature rise within the liquid region was negligible under the studied conditions.[19]

Results and Discussion

Interface force-field parameterization

To assess the performance the Optimized FF, E_{int} was compared to the Original FF and accurate DFT calculations using the optB86b-vdW functional[48,49] for a wide range of configurations. Fig. 4 shows z-scans of E_{int} for LC (flat) (a) and LC (vertical) (b) HAm configurations obtained using DFT calculations, the Original FF, and the Optimized FF. Comparisons of z-scans of E_{int} to the DFT calculations for ClayFF[33] and the FF due Savio et al.[35] are shown in the SI (Fig. S3). In the DFT calculations, adsorption is stronger for the LC (flat) case (E_{ads} = -60.0 kcal mol^{-1}) compared to LC (vertical) (E_{ads} = -48.4 kcal mol^{-1}) conformation owing to vdW interactions between the tailgroups and the surface atoms.[40]

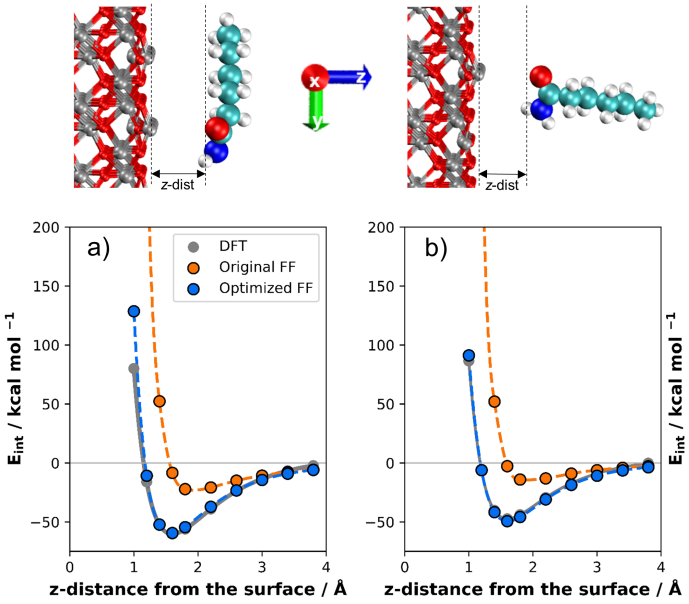

Figure 4: z-Scans of E_{int} for the a) LC (flat) and b) LC (vertical) HAm configurations. Solid gray line is spline interpolation to DFT data, dashed orange line is Original FF,[34] dashed blue line is Optimized FF.

Comparing the Original FF[34] to the DFT calculations, when the HAm molecules are $\geq$ 2.5 Å from the surface and E_{int} is relatively weak, reasonable agreement is achieved for both the LC (flat) and LC (vertical) conformations. However, as the HAm molecules are

moved closer to the surface, the agreement with DFT becomes much poorer. Firstly, the equilibrium adsorption distance, $z_{eq} \approx 1.9$ Å for the Original FF, which is ~ 0.4 Å larger than the 1.5 Å obtained using DFT. Moreover, $E_{ads} \approx$ -20 kcal mol^{-1}, which is much lower than the value obtained from DFT, $E_{ads} \approx$ -50 kcal mol^{-1}. As is commonly observed for LJ potentials,[62,70,83] the repulsive energy at small molecule-surface separations is also considerably overestimated.

Conversely, the Optimized FF shows excellent agreement with the z-scan of E_{int} from the DFT calculations for both the LC (flat) and LC (vertical) HAm conformations. Note that Fig. 4 also includes configurations ≤ 1.0 Å from the surface which were not included in the training dataset. The repulsive energy for these configurations is overestimated as a result of the unphysically steep repulsive term in the 12-6 LJ potential.[62,70,83] However, the overestimation for the Optimized FF is much less severe than for the Original FF. It is noteworthy that the very high energy configurations are unlikely to be accessed in MD simulations and therefore the accuracy of these energies is less important.[62] Nevertheless, the Optimized FF will correctly predict repulsive energies in order to avoid sampling unrealistic configurations in the MD simulations. To match the DFT energies for the closest-ranged configurations, Morse parameters would need to be fit for all of the non-bonded interactions;[83] however, this would complicate the optimization procedure and would risk overfitting.[60,61] Further improvements could perhaps be obtained by using a more computationally expensive polarizable FF[69] rather than the partial charge model employed here for the electrostatic interactions.

Although it was not used in the parameterization, it was also ensured that z-scan for a relaxed n-hexane molecule on α-$Fe_2O_3(0001)$ was accurately reproduced with the Optimized FF. For both the Original FF and Optimized FF, E_{ads} for n-hexane on was underestimated compared to that obtained from the DFT calculations, as shown in the SI (Fig. S6). To improve agreement with the DFT calculations for n-hexane, ϵ_{Fe} could be increased, similar to the approach used by Savio et a.[35] However, this would negatively influence the agreement

of the Optimized FF with the DFT results for the HAm molecules, which was the main aim of this study. Alternatively, improved agreement could be obtained by developing Morse parameters for the interaction of C and H atoms in *n*-hexane with the surface atoms,[83] but this is beyond the scope of this current study.

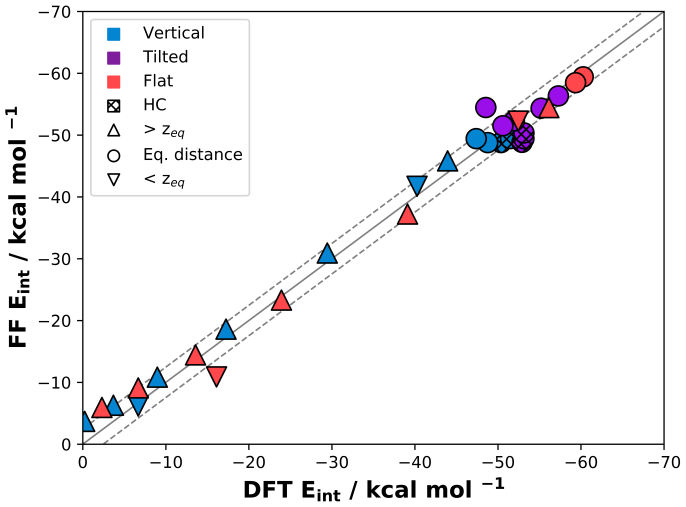

Figure 5: Comparison of the interaction energy, E_{int}, from the Optimized FF and DFT calculations for all of the configurations investigated. Solid line represents perfect fitting, dashed lines represent the RMS error of 2.45 kcal mol^{-1}.

A comparison between the E_{int} values obtained from the Optimized FF and the DFT calculations for all of the configurations included in the parameterization is shown in Fig. 5. The linear fit of these data has an R^2 value of 0.98, representing a dramatic improvement over the Original FF[34] and other alternatives shown in the SI (Fig. S3-4). Overall, the deviations between the FF and DFT energies amount to a root mean square (RMS) error of only 2.5 kcal mol^{-1}, which is an order of magnitude smaller than the strength of the interactions. Thus, the performance of the Optimized FF compares favorably with interface FFs developed for other molecule-surface combinations where direct comparisons between E_{int} from the FF and DFT were conducted.[43,62,64]

Large-scale NEMD simulations

In the final stage, the Optimized FF was compared to the Original FF[34] in large-scale NEMD simulations of amide films adsorbed on α-Fe_2O_3(0001) surfaces at 300 K. Fig. 6 shows number density profiles for the SAm headgroup (amide C, O, H, N) atoms which give indications regarding the orientation of the headgroups. Number density profiles shown for the top wall moving in the $+x$ direction, results for $-x$, $+y$, and $-y$ are shown in the SI (Fig. S7-9).

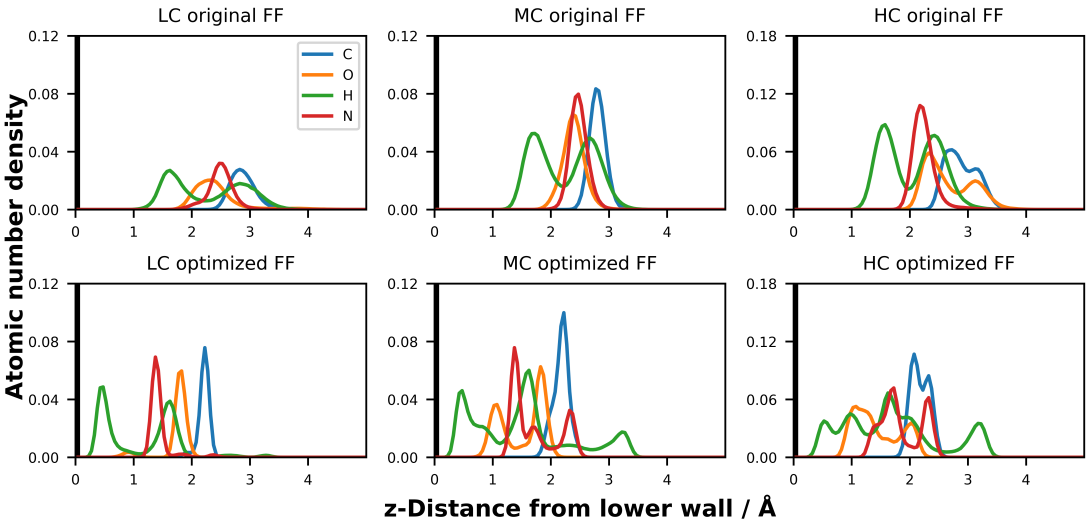

Figure 6: Number density profiles for SAm and n-hexadecane atoms for the Original FF (top) and optimized FF (bottom) under sliding conditions. Top wall moved in the $+x$ direction.

Generally, the atomic number density peaks in Fig. 6 become more intense as the coverage is increased from LC to HC for both the Original FF and the Optimized FF, which is indicative of more ordered molecules. For the Original FF, there are two H_{amide} peaks in Fig. 6 which have similar intensity to each other at LC, MC, and HC. The Original FF also shows single O_{amide} and N_{amide} peaks which are approximately equidistant from the surface at all coverages considered. This is unsurprising since these atoms have similar LJ parameters (σ_O = 2.96 Å, ϵ_O = 0.21 kcal mol^{-1}, σ_N = 3.25 Å, ϵ_N = 0.17 kcal mol^{-1})[24] which govern the interaction strength and distance with the surface atoms. Previous NEMD studies with the Original FF[19] have shown that the SAm tailgroups become more upright as

the coverage is increased. However, these current results suggest that the headgroups remain in a similar conformation as the coverage is increased.

The DFT calculations suggest that the headgroup conformation is actually rather sensitive to surface coverage, as shown in Fig. 2. In the most stable (E_{ads} = -60.4 kcal mol^{-1}) LC (flat) conformation, the two H_{amide} atoms are at a similar z-distance from the surface (within 0.2 Å). In this conformation, both of the H_{amide} atoms H-bond with O_{surf} atoms, as shown in Fig. 3. In the LC (vertical) conformation, which has lower stability (E_{ads} = -48.9 kcal mol^{-1}), two distinct H_{amide}-O_{surf} distances are observed (separated by ¿ 1.0 Å). In this case, only one H_{amide} atom H-bonds with a O_{surf} atom and the vdW interactions between the tailgroup atoms and the surface are much weaker.[40] Two H_{amide}-O_{surf} distances (separated by ¿ 1.0 Å) are also observed at HC (E_{ads} = -51.7 kcal mol^{-1}); one H_{amide} atom H-bonds with a O_{surf} atom, and the other which H-bonds with the O_{amide} atom in a neighbouring molecule, as shown in Fig. 3. It is noteworthy that several almost isoenergetic conformations with slightly different H_{amide}-O_{surf} distances were also observed in the DFT calculations; those included in the paramterization are shown in the SI (Fig. S1). In Fig. 6, the separation between the two H_{amide} peaks $\sim$ 1.0 Åat all coverages for the Original FF. Collectively, this suggests that, when using the Original FF, the SAm headgroups adopt an intermediate conformation between LC (vertical) and LC (flat) (Fig. 2) from DFT, irregardless of the surface coverage.

Fig. 6 shows that the headgroup conformations are rather different when using the Optimized FF, particularly at MC and HC. The headgroup C atom peak is $\sim$ 0.4 Å closer to the surface at all coverages studied for the Optimized FF compared to the Original FF, which corresponds to the shift in z_{eq} shown in Fig. 4. At LC, there are two H_{amide} peaks (separated by $\sim$ 1.0 Å) and single O_{amide} and N_{amide} peaks, with the latter slightly ($\sim$ 0.5 Å) closer to the surface. This suggests an intermediate between the LC (flat) and LC (vertical) conformations shown in Fig. 2 for the Optimized FF at LC, similar to the Original FF. Three separate H_{amide} peaks are observed in Fig. 6 at MC and HC, the middle of which is the most intense and the latter two are separated by ¿ 1.0 Å. There are also two O_{amide} and two

N_{amide} peaks, with the first O_{amide} peak closest to the surface, followed by the first N_{amide} peak. This suggests that two different headgroup conformations are present when using the Optimized FF at MC and HC. One of these conformations is probably the most stable HC system shown in Fig. 2 (E_{ads} = -51.7 kcal mol^{-1}) and the other the HC system shown in the SI (Fig. S1), which is slightly less stable (E_{ads} = -50.5 kcal mol^{-1}). As the coverage increases, there are larger steric interactions between neighboring SAm molecules, which retards molecular rearrangement. Consequently, the SAm molecules are unable to rearrange themselves to reach the lowest E_{ads} conformations at MC and HC, and can become trapped in geometries with slightly lower stability. In summary, the Optimized FF more faithfully reproduces the relaxed DFT conformations shown in Fig. 2 and Fig. S1 in large-scale NEMD simulations.

Fig. 7 shows atomic x-velocity profiles separated into 1.0 Å spatial bins in the z direction, $v_x(z)$. These are overlaid with SAm and n-hexadecane mass density profiles from 0.05 Å spatial bins in z, $\rho(z)$. Profiles for the top wall moving in the $+x$ direction are shown in Fig. 7, profiles for the top wall moving the $-x$, $+y$ and $-y$ directions are shown in the SI (Fig. S10-12).

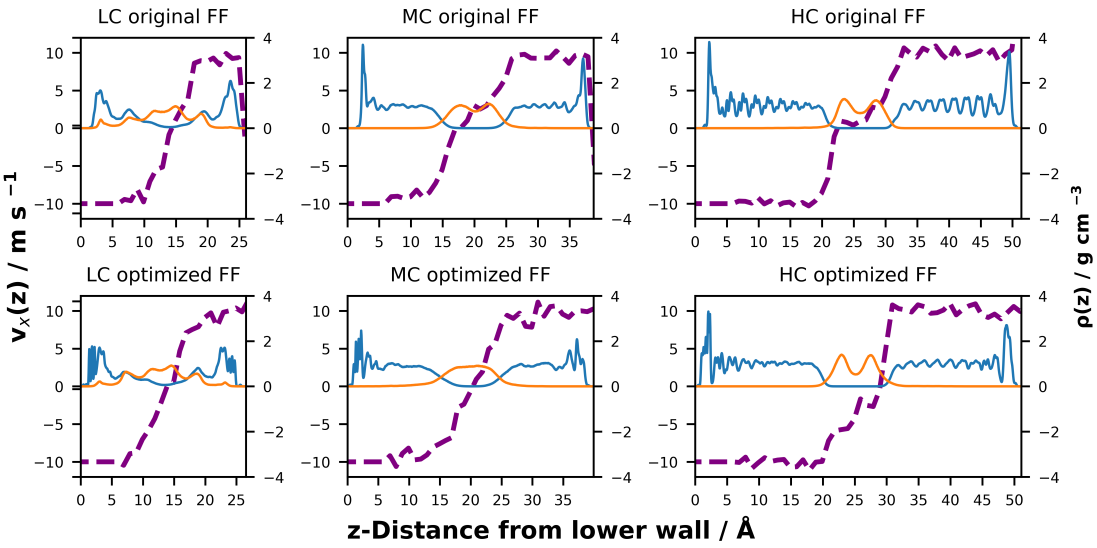

Figure 7: Velocity profiles for atomic velocities along the x direction from 1.0 Å spatial bins in z, $v_x(z)$. SAm and n-hexadecane mass density profiles from 0.05 Å spatial bins in z, $\rho(z)$, are overlaid. Top wall moved in the $+x$ direction.

Fig. 7 suggests that, for all of the coverages studied, the structure and flow behaviour remains broadly similar for the Original FF and the Optimized FF. The mass density profiles show that the SAm films become thicker and show more layering with increasing coverage. Generally, fewer peaks are apparent when using the Optimized FF compared to the Original FF, suggesting less structured, more liquid-like films.[19] The overlap between the SAm and n-hexadecane peaks decreases with increasing coverage, indicating less interdigitation. There is also slightly more interdigitation for the Optimized FF compared to the Original FF. Increased interdigitation has been shown to lead to higher friction in previous NEMD simulations of adsorbed surfactant films.[19,84] Thus, purely from the mass density profiles, friction is expected to decrease with increasing coverage and to be slightly higher for the Optimized FF compared to the Original FF.

The velocity profiles indicate that the SAm headgroups move at the same velocity as the wall to which they are adsorbed. The tailgroups move at the same velocity as the headgroups until the outer region where they interdigitate with the n-hexadecane molecules, at which

point they start to be sheared.[19] At LC, *n*-hexadecane penetrates the entire film, so all but the first strongly adsorbed layer, i.e. the central $\sim$ 15 Åis sheared. Interdigitation occurs $\sim$ 10 Åinto the MC film and the 10 Åthick central region is sheared. At HC, negligible shear occurs because slip planes form between the solid-like SAm films and the *n*-hexadecane lubricant.[19,21] At all coverages, the velocity profiles are essentially indistinguishable between the Original FF and the Optimized FF, suggesting similar flow behaviour.

The friction behaviour was also compared between the Original FF and the Optimized FF, as shown in Fig. 8. The friction coefficient was calculated using the Amontons-Coulomb friction law under the high load approximation: $\mathrm{F}_L/\mathrm{F}_N = \mu + \mathrm{F}_0/\mathrm{F}_N \approx \mu$, where F_L and F_N are respectively the mean lateral (friction) force and normal force acting on the outer layer of atoms in each slab, and F_0 is the load-independent Derjaguin offset representing adhesive surface forces. Previous NEMD simulations have confirmed the applicability of this approximation for OFM films between atomically-smooth surfaces with a separating lubricant layer.[17–19] Points and error bars in Fig. 8 represent the mean and one standard deviation between the steady state friction coefficient from simulations with the top wall moving in the $+x$, $-x$, $+y$, $-y$ directions. This was to improve statistics as well as to account for potential friction anisotropy.[81]

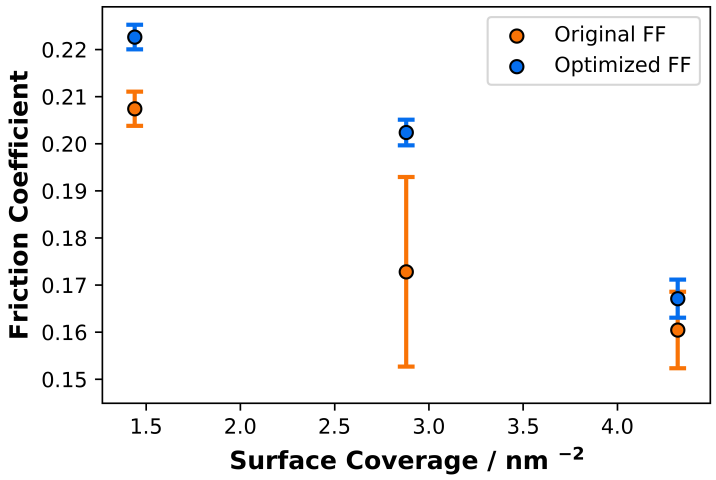

Figure 8: Change in the friction coefficient, μ, with surface coverage for the Original FF compared to the Optimized FF. Circles and error bars represent the mean and one standard deviation between the steady state friction coefficient with the top wall moved the $+x$, -x, $+y$ and -y directions.

For both the Original FF and the Optimized FF, the friction coefficient in Fig. 8 decreases approximately linearly with increasing surface coverage. This is in general agreement with previous NEMD simulations of surfactant-lubricated systems[19,84] as well as atomic force microscopy experiments.[85,86] In macroscopic friction tests, surfactant concentration rather than surface coverage is usually varied since this is much easier to measure and control. However, in boundary friction experiments[15] surfactant molecules with saturated tailgroups, which have been shown to form higher coverage films than those containing Z-unsaturation,[7] gave lower friction. Thus, the friction results in Fig. 8 are in qualitative agreement with trends from nanoscopic[85,86] and macroscopic[15] friction experiments.

The friction coefficients in Fig. 8 are all somewhat higher compared to those reported in Ref.,[19] but these are not directly comparable since the system and conditions are different. In Fig. 8, for all of the coverages studied, the mean friction coefficient is slightly higher for the Optimized FF compared to the Original FF; however, the difference is only statistically significant for the LC and MC cases. This is probably a consequence of the stronger amide-surface binding which leads to more disordered films and increased interdigitation. The

similarity between the FFs is perhaps unsurprising given that the OFM films are preformed on the surfaces (similar to Langmuir-Blodgett experiments)[78] and periodic in the lateral directions, which prevents molecules being squeezed out.[76] Since the molecules cannot leave the contact, the stronger molecule-surface interactions only weakly affect the friction behaviour, which is dominated by the tailgroup interdigitation.[19,84] Therefore, these simulations with the accurate Optimized FF validate the results of previous NEMD studies[17–21] which used the Original FF[34] derived from mixing rules and parameters developed for *n*-alkane adsorption. However, much larger differences between Original FF and Optimized FF are expected for other types of classical MD simulation. For example, the results of nanotribological simulations in which the surfactant molecules can be squeezed out of the contact will be more dependant upon the molecule-surface interaction strength.[76,87] The molecule-surface interaction strength will also affect simulations of surfactant adsorption from nonpolar solvents.[9,88] The Optimized FF developed here will facilitate MD simulations of amides on iron oxide surfaces in which the molecule-surface interactions faithfully reproduce interactions from accurate DFT calculations.

Unlike NEMD simulations of thiol monolayers adsorbed on gold surfaces,[81] no systematic difference in the friction coefficient between the different sliding directions (friction asymmetry) was observed in these simulations. This is probably due to the thin lubricant layer which separates the OFM films.[19] However, the smaller error bars in Fig. 8 indicate that there was less variation in the friction coefficient between the different sliding directions when the Optimized FF was used compared to the Original FF, particularly at MC.

Conclusions

In this study, an Optimized FF was developed for MD simulations of the anhydrous interface between the amide surfactants and iron oxide surfaces. DFT + U calculations using an accurate vdW functional were performed on a wide range of HAm geometries on α-Fe_2O_3(0001)

to ensure extensive sampling of the conformational phase space. The polar amide headgroups strongly chemisorb on the surface and it was found that these interactions could not be accurately represented with a standard LJ potential. Instead, a Morse potential was used for the most strongly interacting molecule-surface atom pairs; O_{amide}-Fe_{surf}, N_{amide}-Fe_{surf}, and H_{amide}-O_{surf}. Different optimization algorithms and constraints were tested, which ultimately yielded excellent agreement between the Optimized FF and the DFT calculations.

The Optimized FF was tested in large-scale NEMD simulations of a thin layer of *n*-hexadecane lubricant confined between amide films with different coverages adsorbed on iron oxide surfaces. The amide molecules were drawn closer to the surface and the orientation of the headgroup was more similar to that observed in the DFT calculations when the Optimized FF was employed. However, for the systems and conditions studied, the velocity profiles and friction coefficient are very similar for the Original FF and the Optimized FF. Since the molecules cannot be squeezed out of the contact, the stronger molecule-surface interactions do not significantly affect the friction behaviour, which is dominated by the tailgroup interdigitation. Therefore, these results validate the findings of previous NEMD studies which used the Original FF derived from mixing rules and parameters developed for *n*-alkane adsorption. The Optimized FF will facilitate MD simulations at the amide-iron oxide interface in which the interactions are representative of those observed in accurate DFT calculations.

Acknowledgement

The authors thank Hongyu Gao, Martin H. Müser, Joshua D. Moore and Joseph Remias for useful discussions. C. A. L. thanks Afton Chemical Corp. and the Engineering and Physical Sciences Research Council (EPSRC) for PhD funding via the Theory and Simulation of Materials-Center for Doctoral Training (TSM-CDT) EP/L015579/1. J. P. E. and D. D. acknowledge the EPSRC for Established Career Fellowship EP/N025954/1 and grant

EP/P030211/1. C. G. is supported by the European Union's Horizon 2020 research and innovation program under the Marie Skodowska-Curie grant agreement No. 744027. We acknowledge the use of Imperial College London Research Computing Service (RCS). All data reported in the manuscript can be obtained by emailing the corresponding author or tribology@imperial.ac.uk.

Supporting Information Available

Supporting Information (SI) includes; additional relaxed DFT configurations, details of the force-field parameterization algorithm, comparisons of the performance different functional forms, tests for *n*-alkane adsorption, and additional results from the molecular dynamics simulations.

This material is available free of charge via the Internet at `http://pubs.acs.org/`.

References

(1) Heinz, H.; Pramanik, C.; Heinz, O.; Ding, Y.; Mishra, R. K.; Marchon, D.; Flatt, R. J.; Estrela-Lopis, I.; Llop, J.; Moya, S. et al. Nanoparticle decoration with surfactants: molecular interactions, assembly, and applications. *Surf. Sci. Rep.* **2017**, *72*, 1–58.

(2) Araujo, A. C.; Viana, P. R. M.; Peres, A. E. C. Reagents in iron ores flotation. *Miner. Eng.* **2005**, *18*, 219–224.

(3) Zhu, Y.; Free, M. L.; Woollam, R.; Durnie, W. A review of surfactants as corrosion inhibitors and associated modeling. *Prog. Mater. Sci.* **2017**, *90*, 159–223.

(4) Spikes, H. Friction Modifier Additives. *Tribol. Lett.* **2015**, *60*, 5.

(5) Holmberg, K.; Erdemir, A. Influence of tribology on global energy consumption, costs and emissions. *Friction* **2017**, *5*, 263–284.

(6) Campen, S.; Green, J. H.; Lamb, G. D.; Spikes, H. A. In Situ Study of Model Organic Friction Modifiers Using Liquid Cell AFM; Saturated and Mono-unsaturated Carboxylic Acids. *Tribol. Lett.* **2015**, *57*, 18.

(7) Wood, M. H.; Casford, M. T.; Steitz, R.; Zarbakhsh, A.; Welbourn, R. J. L.; Clarke, S. M. Comparative Adsorption of Saturated and Unsaturated Fatty Acids at the Iron Oxide/Oil Interface. *Langmuir* **2016**, *32*, 534.

(8) Oh, S. J.; Cook, D. C.; Townsend, H. E. Characterization of iron oxides commonly formed as corrosion products on steel. *Hyperfine Interact.* **1998**, *112*, 59–66.

(9) Jaishankar, A.; Jusufi, A.; Vreeland, J. L.; Deighton, P.; Pellettiere, J. R.; Schilowitz, A. M. Adsorption of stearic acid at the iron oxide/oil interface - theory, experiments and modeling. *Langmuir* **2019**, *35*, 2033–2046.

(10) Sahoo, R. R.; Biswas, S. K. Frictional response of fatty acids on steel. *J. Colloid Interface Sci.* **2009**, *333*, 707–718.

(11) Chernyshova, I. V.; Ponnurangam, S.; Somasundaran, P. Adsorption of Fatty Acids on Iron (Hydr)oxides from Aqueous Solutions. *Langmuir* **2011**, *27*, 10007–10018.

(12) Wood, M. H.; Welbourn, R. J. L.; Charlton, T.; Zarbakhsh, A.; Casford, M. T.; Clarke, S. M. Hexadecylamine Adsorption at the Iron Oxide-Oil Interface. *Langmuir* **2013**, *29*, 13735–13742.

(13) Loehlé, S.; Matta, C.; Minfray, C.; Le Mogne, T.; Iovine, R.; Obara, Y.; Miyamoto, A.; Martin, J.-M. Mixed lubrication of steel by C18 fatty acids revisited. Part I: toward the formation of carboxylate. *Tribol. Int.* **2015**, *82*, 218–227.

(14) Ruths, M.; Lundgren, S.; Danerlov, K.; Persson, K. Friction of fatty acids in nanometer-sized contacts of different adhesive strength. *Langmuir* **2008**, *24*, 1509–1516.

(15) Campen, S.; Green, J.; Lamb, G.; Atkinson, D.; Spikes, H. On the increase in boundary friction with sliding speed. *Tribol. Lett.* **2012**, *48*, 237–248.

(16) Ewen, J. P.; Heyes, D. M.; Dini, D. Advances in nonequilibrium molecular dynamics simulations of lubricants and additives. *Friction* **2018**, *6*, 349–386.

(17) Doig, M.; Warrens, C. P.; Camp, P. J. Structure and friction of stearic acid and oleic acid films adsorbed on iron oxide surfaces in squalane. *Langmuir* **2014**, *30*, 186–195.

(18) Doig, M.; Camp, P. J. The structures of hexadecylamine films adsorbed on iron-oxide surfaces in dodecane and hexadecane. *Phys. Chem. Chem. Phys.* **2015**, *17*, 5248–5255.

(19) Ewen, J. P.; Gattinoni, C.; Morgan, N.; Spikes, H. A.; Dini, D. Nonequilibrium Molecular Dynamics Simulations of Organic Friction Modifiers Adsorbed on Iron Oxide Surfaces. *Langmuir* **2016**, *32*, 4450.

(20) Ewen, J. P.; Gattinoni, C.; Thakkar, F. M.; Morgan, N.; Spikes, H.; Dini, D. A Comparison of Classical Force-Fields for Molecular Dynamics Simulations of Lubricants. *Materials.* **2016**, *9*, 651.

(21) Ewen, J. P.; Kannam, S. K.; Todd, B. D.; Dini, D. Slip of alkanes confined between surfactant monolayers adsorbed on solid surfaces. *Langmuir* **2018**, *34*, 3864–3873.

(22) Allen, W.; Rowley, R. L. Predicting the viscosity of alkanes using nonequilibrium molecular dynamics: Evaluation of intermolecular potential models. *J. Chem. Phys.* **1997**, *106*, 10273–10281.

(23) Harrison, J. A.; Schall, J. D.; Maskey, S.; Mikulski, P. T.; Knippenberg, M. T.; Morrow, B. H. Review of force fields and intermolecular potentials used in atomistic computational materials research. *Appl. Phys. Rev.* **2018**, *5*, 031104.

(24) Jorgensen, W. L.; Maxwell, D. S.; Tirado-Rives, J. Development and testing of the

OPLS all-atom force field on conformational energetics and properties of organic liquids. *J. Am. Chem. Soc.* **1996**, *118*, 11225–11236.

(25) Price, M. L. P.; Ostrovsky, D.; Jorgensen, W. L. Gas-phase and liquid-state properties of esters, nitriles, and nitro compounds with the OPLS-AA force field. *J. Comput. Chem.* **2001**, *22*, 1340–1352.

(26) Siu, S. W. I.; Pluhackova, K.; Bockmann, R. A. Optimization of the OPLS-AA Force Field for Long Hydrocarbons. *J. Chem. Theory Comput.* **2012**, *8*, 1459–1470.

(27) Wang, J. M.; Wolf, R. M.; Caldwell, J. W.; Kollman, P. A.; Case, D. A. Development and testing of a general amber force field. *J. Comput. Chem.* **2004**, *25*, 1157–1174.

(28) Vanommeslaeghe, K.; Hatcher, E.; Acharya, C.; Kundu, S.; Zhong, S.; Shim, J.; Darian, E.; Guvench, O.; Lopes, P.; Vorobyov, I. et al. CHARMM General Force Field: A Force Field for Drug-Like Molecules Compatible with the CHARMM All-Atom Additive Biological Force Fields. *J. Comput. Chem.* **2010**, *31*, 671–690.

(29) Sun, H.; Jin, Z.; Yang, C.; Akkermans, R. L.; Robertson, S. H.; Spenley, N. A.; Miller, S.; Todd, S. M. COMPASS II: extended coverage for polymer and drug-like molecule databases. *J. Mol. Model.* **2016**, *22*, 1–10.

(30) Herbers, C. R.; Li, C.; van der Vegt, N. F. A. Grand Challenges in Quantum-Classical Modeling of Molecule- Surface Interactions. *J. Comput. Chem.* **2013**, *34*, 1177–1188.

(31) Lennard-Jones, J. E. On the determination of molecular fields.-II. From the equation of state of a gas. *Proc. R. Soc. Lond. A* **1924**, *106*, 463–477.

(32) Heinz, H.; Lin, T. J.; Kishore Mishra, R.; Emami, F. S. Thermodynamically consistent force fields for the assembly of inorganic, organic, and biological nanostructures: The INTERFACE force field. *Langmuir* **2013**, *29*, 1754–1765.

(33) Cygan, R. T.; Liang, J. J.; Kalinichev, A. G. Molecular models of hydroxide, oxyhydroxide, and clay phases and the development of a general force field. *J. Phys. Chem. B* **2004**, *108*, 1255–1266.

(34) Berro, H.; Fillot, N.; Vergne, P. Molecular dynamics simulation of surface energy and ZDDP effects on friction in nano-scale lubricated contacts. *Tribol. Int.* **2010**, *43*, 1811–1822.

(35) Savio, D.; Fillot, N.; Vergne, P.; Zaccheddu, M. A Model for Wall Slip Prediction of Confined n-Alkanes: Effect of Wall-Fluid Interaction Versus Fluid Resistance. *Tribol. Lett.* **2012**, *46*, 11–22.

(36) Carrasco, J.; Liu, W.; Michaelides, A.; Tkatchenko, A. Insight into the description of van der Waals forces for benzene adsorption on transition metal (111) surfaces. *J. Chem. Phys.* **2014**, *140*, 084704.

(37) Murphy, C. J.; Carrasco, J.; Lawton, T. J.; Liriano, M. L.; Baber, A. E.; Lewis, E. A.; Michaelides, A.; Sykes, E. C. H. Structure and energetics of hydrogen-bonded networks of methanol on close packed transition metal surfaces. *J. Chem. Phys.* **2014**, *141*, 014701.

(38) Bedolla, P. O.; Feldbauer, G.; Wolloch, M.; Eder, S. J.; Dorr, N.; Mohn, P.; Redinger, J.; Vernes, A. Effects of van der Waals Interactions in the Adsorption of Isooctane and Ethanol on Fe(100) Surfaces. *J. Phys. Chem. C* **2014**, *118*, 17608–17615.

(39) Gattinoni, C.; Michaelides, A. Understanding corrosion inhibition with van der Waals DFT methods: The case of benzotriazole. *Faraday Discuss.* **2015**, *180*, 439–458.

(40) Gattinoni, C.; Ewen, J. P.; Dini, D. Adsorption of Surfactants on α-Fe2O3(0001): A Density Functional Theory Study. *J. Phys. Chem. C* **2018**, *122*, 20817–20826.

(41) Larrucea, J.; Lid, S.; Colombi Ciacchi, L. Parametrization of a classical force field for iron oxyhydroxide/water interfaces based on Density Functional Theory calculations. *Comput. Mater. Sci.* **2014**, *92*, 343–352.

(42) Ta, T. D.; Tieu, A. K.; Zhu, H.; Kosasih, B. Adsorption of Normal-Alkanes on Fe(110), FeO(110), and Fe2O3(0001): Influence of Iron Oxide Surfaces. *J. Phys. Chem. C* **2015**, *119*, 12999–13010.

(43) Tromp, S.; Joly, L.; Cobian, M.; Fillot, N. Chemical Physics at Interfaces within a Refrigerant-Lubricated Contact: From Electronic Structure to Large-Scale Molecular Dynamics Simulations. *J. Phys. Chem. C* **2018**, *122*, 5420–5429.

(44) Kresse, G.; Hafner, J. Ab initio molecular dynamics for liquid metals. *Phys. Rev. B* **1993**, *47*, 558.

(45) Kresse, G.; Furthmuller, J. Efficiency of ab-initio total energy calculations for metals and semiconductors using a plane-wave basis set. *Comput. Mater. Sci.* **1996**, *6*, 15–50.

(46) Kresse, G.; Furthmuller, J. Efficient iterative schemes for ab initio total-energy calculations using a plane-wave basis set. *Phys. Rev. B* **1996**, *54*, 11169.

(47) Kresse, G.; Joubert, D. From ultrasoft pseudopotentials to the projector augmented-wave method. *Phys. Rev. B.* **1999**, *59*, 1758–1775.

(48) Klimeš, J.; Bowler, D. R.; Michaelides, A. Chemical accuracy for the van der Waals density functional. *J. Phys. Condens. Matter* **2010**, *22*.

(49) Klimeš, J.; Bowler, D. R.; Michaelides, A. Van der Waals density functionals applied to solids. *Phys. Rev. B* **2011**, *83*, 195131.

(50) Dudarev, S.; Botton, G. Electron-energy-loss spectra and the structural stability of nickel oxide: An LSDA+U study. *Phys. Rev. B* **1998**, *57*, 1505–1509.

(51) Huang, X.; Ramadugu, S. K.; Mason, S. E. Surface-Specific DFT + U Approach Applied to α-Fe2O3(0001). *J. Phys. Chem. C* **2016**, *120*, 4919–4930.

(52) Makov, G.; Payne, M. Periodic boundary conditions in ab initio calculations. *Phys. Rev. B* **1995**, *51*, 4014–4022.

(53) Humphrey, W.; Dalke, A.; Schulten, K. VMD: Visual molecular dynamics. *J. Mol. Graph. Model.* **1996**, *14*, 33–38.

(54) Parkinson, G. S. Iron oxide surfaces. *Surf. Sci. Rep.* **2016**, *71*, 272–365.

(55) Yamamoto, S.; Kendelewicz, O. T.; Newberg, J. T.; Ketteler, G.; Starr, D. E.; Mysak, E. R.; Andersson, K. J.; Ogasawara, H.; Bluhm, H.; Salmeron, M. et al. Water Adsorption on a-Fe2O3 (0001) at near Ambient Conditions. *J. Phys. Chem. C* **2010**, *114*, 2256–2266.

(56) Lancaster, J. K. A review of the influence of environmental humidity and water on friction, lubrication and wear. *Tribol. Int.* **1990**, *23*, 371–389.

(57) Wilson, D.; Langell, M. A. XPS analysis of oleylamine/oleic acid capped Fe3O4 nanoparticles as a function of temperature. *Appl. Surf. Sci.* **2014**, *303*, 6–13.

(58) Filius, J. D.; Hiemstra, T.; Riemsdijk, W. H. V. Adsorption of Small Weak Organic Acids on Goethite: Modeling of Mechanisms. *J. Colloid Interface Sci.* **1997**, *380*, 368–380.

(59) Tsuzuki, S.; Honda, K.; Uchimaru, T.; Mikami, M. Magnitude of interaction between n-alkane chains and its anisotropy: High-level ab initio calculations of n-butane, n-petane, and n-hexane dimers. *J. Phys. Chem. A* **2004**, *108*, 10311–10316.

(60) Gao, D. Z.; Federici Canova, F.; Watkins, M. B.; Shluger, A. L. Efficient parametrization of complex molecule-surface force fields. *J. Comput. Chem.* **2015**, *36*, 1187–1195.

(61) Huan, T. D.; Batra, R.; Chapman, J.; Krishnan, S.; Chen, L.; Ramprasad, R. A universal strategy for the creation of machine learning-based atomistic force fields. *npj Comput. Mater.* **2017**, *3*, 37.

(62) Johnston, K.; Herbers, C. R.; Van Der Vegt, N. F. Development of classical molecule-surface interaction potentials based on density functional theory calculations: Investigation of force field representability. *J. Phys. Chem. C* **2012**, *116*, 19781–19788.

(63) Bamdad, M.; Farrokhpour, H.; Ashrafizaadeh, M. A new force field for the adsorption of H2, O2, N2, CO, H2O, and H2S gases on alkali doped carbon nanotubes. *Mol. Phys.* **2016**, *114*, 3375–3387.

(64) Berg, A.; Peter, C.; Johnston, K. Evaluation and Optimization of Interface Force Fields for Water on Gold Surfaces. *J. Chem. Theory Comput.* **2017**, *13*, 5610–5623.

(65) Bolton, K.; Bosio, S.; Hase, W. L.; Schneider, W. F.; Hass, K. C. Comparison of Explicit and United Atom Models for Alkane Chains Physisorbed on α-Al2O3 (0001). *J. Phys. Chem. B* **1999**, *103*, 3885–3895.

(66) Plimpton, S. Fast Parallel Algorithms for Short-Range Molecular Dynamics. *J. Comput. Phys.* **1995**, *117*, 1 – 19.

(67) Yeh, I. C.; Berkowitz, M. L. Ewald summation for systems with slab geometry. *J. Chem. Phys.* **1999**, *111*, 3155–3162.

(68) Poli, R.; Kennedy, J.; Blackwell, T. Particle swarm optimization: An overview. *Swarm Intell.* **2007**, *1*, 33–57.

(69) Wang, L.-P.; Chen, J.; Van Voorhis, T. Systematic Parametrization of Polarizable Force Fields from Quantum Chemistry Data. *J. Chem. Theory Comput.* **2013**, *9*, 452–460.

(70) Kong, L. T.; Denniston, C.; Müser, M. H.; Qi, Y. Non-bonded force field for the

interaction between metals and organic molecules: a case study of olefins on aluminum. *Phys. Chem. Chem. Phys.* **2009**, *11*, 10195–10203.

(71) Ercolessi, F.; Adams, J. Interatomic Potentials From First-Principles Calculations: The Force-Matching Method. *Europhys. Lett.* **1994**, *26*, 583–588.

(72) Morse, P. Diatomic Molecules According to the Wave Mechanics. II. Vibrational Levels. *Phys. Rev.* **1929**, *34*, 57.

(73) Mahaffy, R.; Bhatia, R.; Garrison, B. J. Diffusion of a Butanethiolate Molecule on a Au{111} Surface. *J. Phys. Chem. B* **1997**, *101*, 771–773.

(74) Ahn, Y.; Saha, J. K.; Schatz, G. C.; Jang, J. Molecular Dynamics Study of the Formation of a Self-Assembled Monolayer on Gold. *J. Phys. Chem. C* **2011**, *115*, 10668–10674.

(75) Dixon, D. A.; Dobbs, K. D.; Valentini, J. J. Amide-Water and Amide-Amide Hydrogen Bond Strengths. *J. Phys. Chem.* **1994**, *98*, 13435–13439.

(76) Tartaglino, U.; Sivebaek, I. M.; Persson, B. N. J.; Tosatti, E. Impact of molecular structure on the lubricant squeeze-out between curved surfaces with long range elasticity. *J. Chem. Phys.* **2006**, *125*, 014704.

(77) Ryckaert, J. P.; Ciccotti, G.; Berendsen, H. J. C. Numerical-integration of Cartesian equations of motion of a system with constraints: molecular-dynamics of n-alkanes. *J. Comput. Phys.* **1977**, *23*, 327–341.

(78) Briscoe, B. J.; Evans, D. C. B. The shear properties of Langmuir-Blodgett layers. *Proc. R. Soc. Lond. A* **1982**, *380*, 389.

(79) Ramachandran, S.; Tsai, B. L.; Blanco, M.; Chen, H.; Tang, Y. C.; Goddard, W. A. Self-assembled monolayer mechanism for corrosion inhibition of iron by imidazolines. *Langmuir* **1996**, *12*, 6419–6428.

(80) Schneider, T.; Stoll, E. Molecular-dynamics study of a three-dimensional one-component model for distortive phase-transitions. *Phys. Rev. B* **1978**, *17*, 1302–1322.

(81) Jabbarzadeh, A. Friction anisotropy and asymmetry in self assembled monolayers. *Tribol. Int.* **2016**, *102*, 600–607.

(82) Bernardi, S.; Todd, B. D.; Searles, D. J. Thermostating highly confined fluids. *J. Chem. Phys.* **2010**, *132*, 244706.

(83) O'Connor, T. C.; Andzelm, J.; Robbins, M. O. AIREBO-M: A reactive model for hydrocarbons at extreme pressures. *J. Chem. Phys.* **2015**, *142*, 024903.

(84) Kong, Y. C.; Tildesley, D. J.; Alejandre, J. The molecular dynamics simulation of boundary-layer lubrication. *Mol. Phys.* **1997**, *92*, 7–18.

(85) Lee, S.; Shon, Y.-S.; Colorado, R.; Guenard, R. L.; Lee, T. R.; Perry, S. S. The Influence of Packing Densities and Surface Order on the Frictional Properties of Alkanethiol Self-Assembled Monolayers (SAMs) on Gold: A Comparison of SAMs Derived from Normal and Spiroalkanedithiols. *Langmuir* **2000**, 2220–2224.

(86) Flater, E. E.; Ashurst, W. R.; Carpick, R. W. Nanotribology of octadecyltrichlorosilane monolayers and silicon: Self-mated versus unmated interfaces and local packing density effects. *Langmuir* **2007**, *23*, 9242–9252.

(87) Summers, A. Z.; Iacovella, C. R.; Cummings, P. T.; McCabe, C. Investigating Alkylsilane Monolayer Tribology at a Single-Asperity Contact with Molecular Dynamics Simulation. *Langmuir* **2017**, *33*, 11270–11280.

(88) Bradley-Shaw, J. L.; Camp, P. J.; Dowding, P. J.; Lewtas, K. Molecular Dynamics Simulations of Glycerol Monooleate Confined between Mica Surfaces. *Langmuir* **2016**, *32*, 7707–7718.

Graphical TOC Entry